Int. J. Electrochem. Sci., 15 **(2020)** 5220 – 5231, doi: 10.20964/2020.06.38

International Journal of ELECTROCHEMICAL SCIENCE
www.electrochemsci.org

Fotodeposition of Bimetallic Au-Pt Nanoparticles on the Electrodeposited TiO_2 Nanotube Arrays for Efficient Visible Light-Driven Photocatalytic Performance

Zhenxia Xu[1], *Da Chen*[1,*], *Qiaoli Huang*[1], *Wenlong Song*[2], *Junhui Liang*[1], *Laishun Qin*[1], *Yuexiang Huang*[1,*]

[1] College of Materials and Chemistry, China Jiliang University, Hangzhou, Zhejiang 310018, China
[2] Tianneng Battery Group Co., Ltd., Changxing City, Zhejiang 313100, China
[*]E-mail: dchen_80@hotmail.com, yuexiang65@hotmail.com

Received: 15 January 2020/ *Accepted:* 8 March 2020 / *Published:* 10 May 2020

In this work, well-ordered TiO_2 nanotube arrays (TNTAs) were successfully prepared by a facile electrochemical anodization, and the Au-Pt bimetallic nanoparticles were then deposited on the TNTAs surface for improving their photocatalytic properties. The experimental results reveal that the Au-Pt nanoparticles with the size of ~2 nm were well distributed on the surface of TNTAs, and the Schottky heterojunction was formed at the interface between the Au-Pt nanoparticles and TNTAs. Compared to the pristine TNTAs and monometallic Au/TNTAs or Pt/TNTAs, the Au-Pt/TNTAs exhibited significantly improved photocatalytic activities for rhodamine B (RhB) degradation. The photocatalytic degradation rate constant (k) of the Au-Pt/TNTAs was calculated to be ca. 1.0884 h^{-1}, which was about 3.7 times that of TNTAs and was also greater than the sum of the Au/TNTAs and Pt/TNTAs. The enhanced photocatalytic activities could be ascribed to the synergistic effects of Au-Pt/TNTAs: (1) the largely improved optical absoprtion abilities induced by the surface plasma effect of Au-Pt nanoparticles, and (2) the accelerated separation and migration process of photogenerated carriers arising from the Schottky heterojunction at the interface between Au-Pt and TNTAs.

Keywords: TiO_2 nanotube arrays (TNTAs); Bimetallic Au-Pt nanoparticles; Schottky heterojunction; Photocatalytic performance; Photocatalytic mechanism

1. INTRODUCTION

In the past decades, TiO_2 has been widely used in the field of heterogeneous photocatalysis, e.g., photocatalytic hydrogen production [1], air and water purification [2], photocatalytic CO_2 reduction [3], due to its good stability, low cost and nontoxicity [4]. Particularly, the highly-ordered TiO_2 nanotube arrays (TNTAs) prepared by electrochemical anodization have attracted much more attention, on account of their unique one-dimensional tubular nanostructure, large surface specific area,

good mechanical strength and close contact with the medium [5-7]. However, the intrinsic band gap of TNTAs is ~3.2 eV, which allows its photon absorption only in the ultraviolet region ($\lambda \leq 380$ nm) accounting for only ~4% of the sunlight, thus limiting the utilization of TNTAs. Meanwhile, the easy recombination of photogenerated electrons and holes in TNTAs as well as the relatively poor photocatalytic activity of the bare TNTAs also greatly restrict their photoelectrochemical applications. To address these issues, several approaches, such as dye sensitization [8, 9], metal ion doping [10], heterostructure formation by coupling with other semiconductor nanomaterials [11], and cocatalysts deposition [12, 13], have been proposed. Among these approaches, the deposition of noble metal cocatalysts has been proven as one of the most simple but efficient methods to suppress the recombination of photogenerated electron-hole pairs and expand the spectral absorption range, thus resulting in the enhanced photocatalytic activities of TNTAs.

So far, most of the reported precious metal deposition processes are monometallic deposition, while the bimetallic deposition processes are rare. Compared with the monometallic deposition, however, the bimetallic deposition based on two different metallic co-catalysts can improve the photocatalytic activity to the greatest extent by utilizing the synergistic effect between the two different precious metals [14-17]. For example, Gallo et al. [14] reported the preparation of the Au-Pt bimetallic supported on TiO_2 particles for highly efficient hydrogen production activity, which was much higher than the Pt or Au monometallic supported TiO_2 and the pristine TiO_2 particles. The superior photocatalytic activity of the Au-Pt/TiO_2 was ascribed to the significantly improved visible light absorption, the accelerated charge separation and transfer as well as the suppressed electron-hole recombination process arising from the synergistic effect of Au-Pt bimetallic system. To the best of our knowledge, however, only a few bimetallic systems, namely Cu-Pt nanoparticles [18] and Pd-Ag nanoparticles [19], have been immobilized on TNTAs for photocatalytic applications.

Herein, the loading of bimetallic Au-Pt nanoparticles was employed to improve the photocatalytic performance of TNTAs prepared by electrochemical anodization. Meanwhile, the photocatalytic mechanism for enhanced photocatalytic activities of Au-Pt/TNTAs was also discussed.

2. EXPERIMENTAL DETAILS

2.1 Preparation of TiO_2 nanotube arrays

The TNTAs were prepared by using an electrochemical anodization process, which was performed in a two-electrode electrolytic cell with the pretreated Ti foil as the working electrode and Pt wire as the counter electrode in a mixture electrolyte of glycerol (50%, v/v) and deionized water (50%, v/v) containing NH_4F under constant potential according to the literature [13, 20]. After the anodization, the obtained sample was rinsed with ethanol and then dried in air. Subsequently, the anodized sample was annealed at 450 ^oC for 3 h in oxygen atmosphere with a ramping rate of 2 ^oC/min in a muffle furnace, and was finally cooled to room temperature.

2.2 Preparation of Au-Pt/TNTAs

The Au-Pt/TNTAs photocatalyst was prepared by photodeposition of the bimetallic Au-Pt nanoparticles on the surface of TNTAs through a facile photoreduction method. Typically, the Au-Pt/TNTAs photocatalyst was prepared as follows. Firstly, the above-obtained TNTAs sample was soaked in the precursor solution (4 mM of $HAuCl_4 \cdot 3H_2O$ and 4 mM of $H_2PtCl_6 \cdot 6H_2O$ in methanol/H_2O (1:4 v/v)) overnight in dark. The TNTAs sample was then removed from the precursor solution, and subsequently irradiated by a 500 W high pressure mercury lamp for 30 min for photoreduction. Lastly, the irradiated sample was washed twice with ethanol to remove unadsorbed materials, and then thermally treated at 200 ^oC in vacuum for 4 h in order to improve the adhesion of bimetallic Au-Pt nanoparticles on the surface of TNTAs. Thus, the Au-Pt/TNTAs photocatalyst was obtained. For comparison, the monometallic Au or Pt nanoparticles supported on the surface of TNTAs (i.e., Au/TNTAs, Pt/TNTAs) was also prepared through the same photoreduction process except using different precursor solutions, that is, 4 mM of $HAuCl_4 \cdot 3H_2O$ in methanol/H_2O (1:4 v/v) for Au/TNTAs and 4 mM of $H_2PtCl_6 \cdot 6H_2O$ in methanol/H_2O (1:4 v/v) for Pt/TNTAs.

2.3 Materials Characterizations

The crystal structures of the prepared samples were examined by using a Bruker D2 X-ray diffractometer with Cu K_α radiation (λ = 1.54056 Å) in the 2θ range of 20º~80º. The morphological and elemental analysis of the obtained samples were performed on the field emission scanning electron microscope (Hitachi SU 8010) attached with Energy Dispersive Spectrometer (TEAM Apollo XL EDS, USA). The microstructures of the obtained samples were further investigated by a field-emission transmission electron microscope (TEM, JEOL JEM 2100). For the TEM measurement, the prepared nanotube arrays were carefully peeled off from the Ti substrate and ultrasonically dispersed in alcohol for 30 min, followed by dropping the dispersion onto a copper mesh. The UV-vis diffuse reflectance spectra (DRS) of the samples were measured using a UV 3600 UV-Vis spectrophotometer equipped with an integrating sphere accessory. Photoluminescence (PL) spectra of the samples were carried out using a FL3-211 fluorescence spectrometer (Jobin Yvon, France) at an excitation wavelength of 370 nm.

2.4 Photocatalytic measurements

The photocatalytic activities of the obtained samples were evaluated by photocatatalytic degradation of rhodamine B (RhB). The obtained photocatalysts (TNTAs, Au/TNTAs, Pt/TNTAs, or Au-Pt/TNTAs) were cut to a certain size (1 cm by 1 cm) and placed in a photocatalytic reactor containing a RhB aqueous solution (5 mg L^{-1}). The photocatalytic degradation was then performed under visible light ($\lambda \geq 420$ nm) irradiation from a 100 W Xenon light source assembled with a optical filter with an average intensity of 20 mW cm^{-2}. The distance between the sample and the lamp source was 15 cm. Before irradiation, the reactor was placed in the dark for 30 min to establish the adsorption-desorption equilibrium between the catalyst sample and RhB dye. At regular intervals of

irradiation time, the absorbance of the RhB solution in the reactor was measured at a wavelength of 554 nm (the maximum absorption band for RhB) by using a UV–vis spectrophotometer (Puxi, TU-1901, China).

3. RESULTS AND DISCUSSION

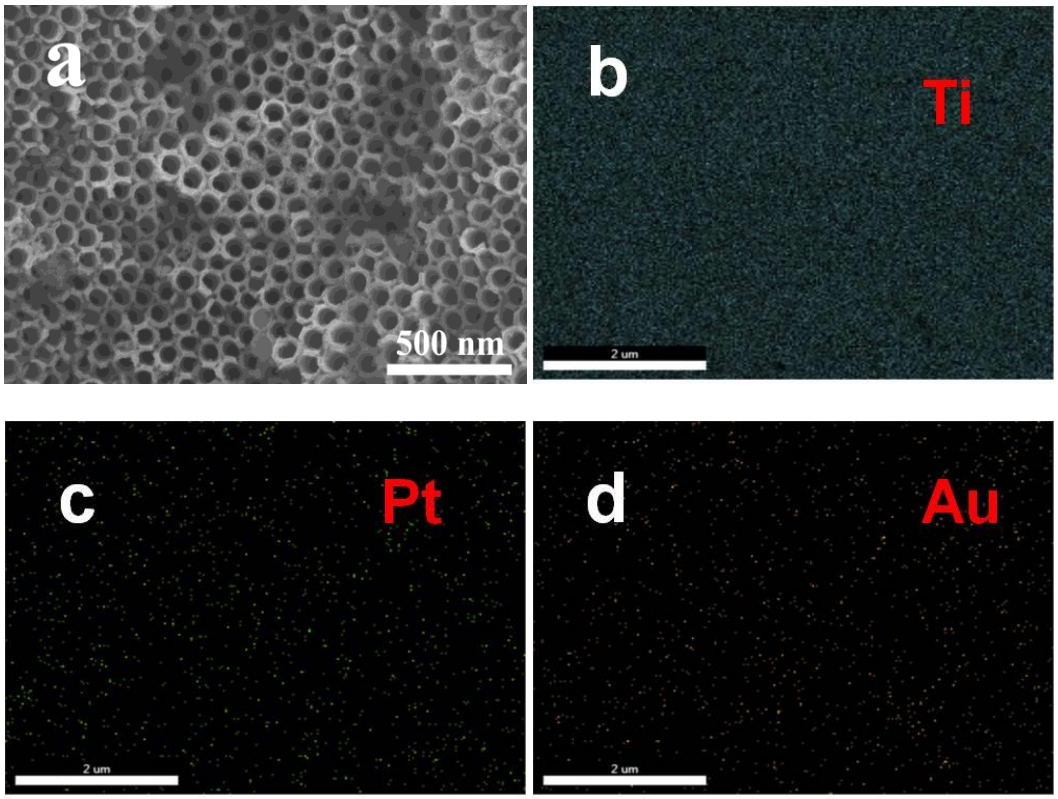

Figure 1. FESEM image of the prepared (a) Au-Pt/TNTAs, and the EDS mapping images of the Au-Pt/TNTAs for (b) Ti, (c) Pt, and (d) Au elements.

Figure 1 shows the FESEM and EDS mapping images of the prepared Au-Pt/TNTAs. As shown in Figure 1a, the TNTAs grown on the titanium sheet were vertically aligned, and the diameter of the nanotubes was in the range of 110-130 nm. The highly ordered TNTAs could possess a very large specific surface area, which could provide a large specific surface area for supporting cocatalysts loading or reactive sites. From FESEM images, it is difficult to observe the Au-Pt nanoparticles on the surface of TNTAs probably because of the small particle size. Nevertheless, the EDS mapping results (Figure 1b-d) clearly reveal that Au and Pt elements were uniformly dispersed on the surface of the TNTAs. Table 1 summarizes the EDS data of the prepared TNTAs, Au/TNTAs, Pt/TNTAs and Au-Pt/TNTAs samples.

Table 1. The EDS data of the prepared TNTAs, Au/TNTAs, Pt/TNTAs, and Au-Pt/TNTAs.

Sample	Element	Weight %	Atomic %
TNTAs	O K	31.14	57.52
	Ti K	68.86	42.48
	Au K	0	0
	Pt K	0	0
Au/TNTAs	O K	31.78	58.47
	Ti K	67.36	41.4
	Au K	0.87	0.13
	Pt K	0	0
Pt/TNTAs	O K	28.27	54.25
	Ti K	71.24	45.67
	Au K	0	0
	Pt K	0.49	0.08
Au-Pt/TNTAs	O K	28.57	54.78
	Ti K	70.36	45.06
	Au K	0.6	0.09
	Pt K	0.47	0.07

As can be seen from Table 1, the ratio of Ti to O atoms in all the prepared samples was much higher than 1:2, which could be ascribed to the fact that all the samples were fabricated on the base of Ti sheets. For both the monometallic and bimetallic loaded samples, the loading amount of metal nanoparticles on the surface of TNTAs was relatively small. With respect to the Au-Pt/TNTAs, the loading amounts of Au and Pt nanoparticles were estimated to be about 0.87% and 0.47 %, respectively.

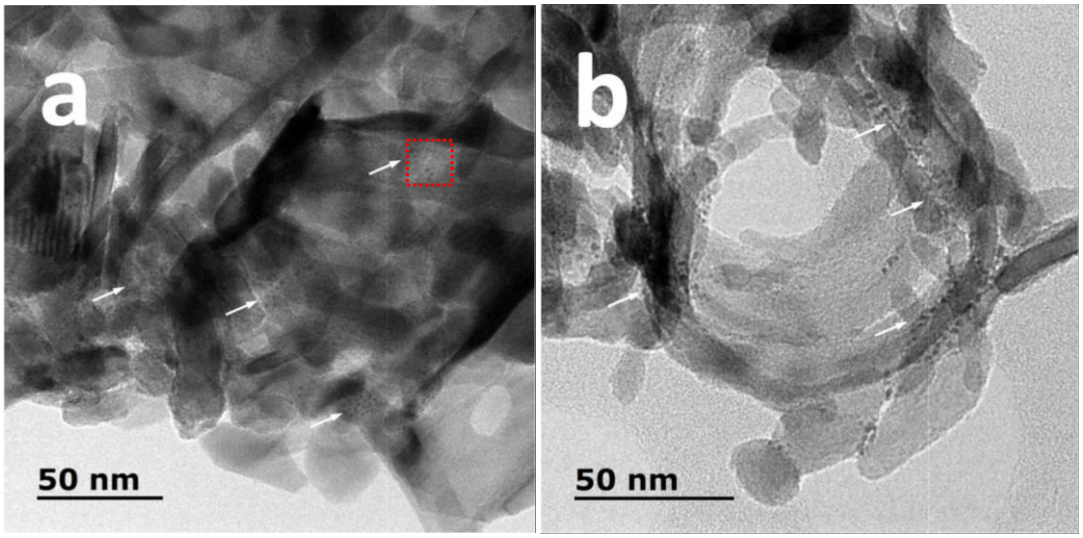

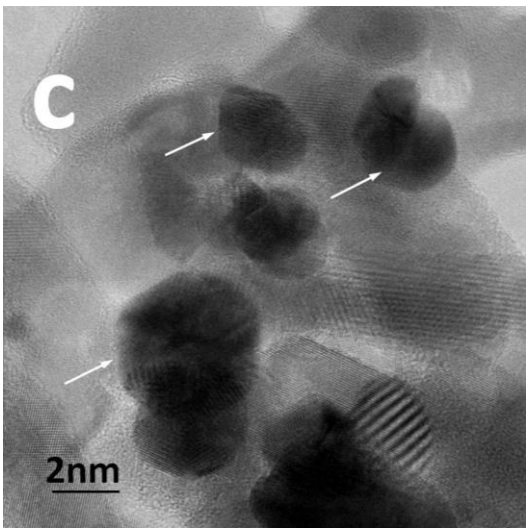

Figure 2. TEM images of the prepared Au-Pt/TNTAs: (a) measured at the area of tube walls (Au-Pt nanoparticles indicated by the arrows), (b) measured at the area of tube mouth (Au-Pt nanoparticles indicated by the arrows), and (c) the HRTEM image of the zone marked with the red dotted box in pattern a.

In order to further investigate the microstructural features of the prepared Au-Pt/TNTAs, the TEM measurements were also performed, as shown in Figure 2. It can be seen that the Au-Pt bimetallic nanoparticles were uniformly attached to both the tube wall (Figure 2a) and the tube mouth (Figure 2b) of the TNTAs, and the Au-Pt nanoparticles were around 2 nm in size (Figure 2c). More importantly, the close contact between the Au-Pt nanoparticles and TNTAs (Figure 2c) would thus form the Schottky heterojunction at the interface between Au-Pt and TNTAs, which could facilitate the separation and migration of photogenerated carriers [21, 22]. Figure 3 shows the XRD patterns of the prepared TNTAs, Au/TNTAs, Pt/TNTAs and Au-Pt/TNTAs. As shown, all the samples had similar XRD patterns, in which four characteristic peaks appearing in $2\theta = 25.5°$, 37.3°, 48.2° and 63.5° could be indexed to the (101), (004), (200), and (204) crystal faces of phase-pure anatase TiO_2 (JCPDS No. 21-1272), respectively, and the other characteristic diffraction peaks were assigned to the Ti substrate (JCPDS 44-1294) [13, 23]. This means that TNTAs were successfully prepared on the Ti substrate. For the Au/TNTAs, Pt/TNTAs or Au-Pt/TNTAs sample, the characteristic peaks of precious metal Au or Pt were not observed probably due to the low loading amount of monometallic or bimetallic nanoparticles below the detection limit of the XRD instrument.

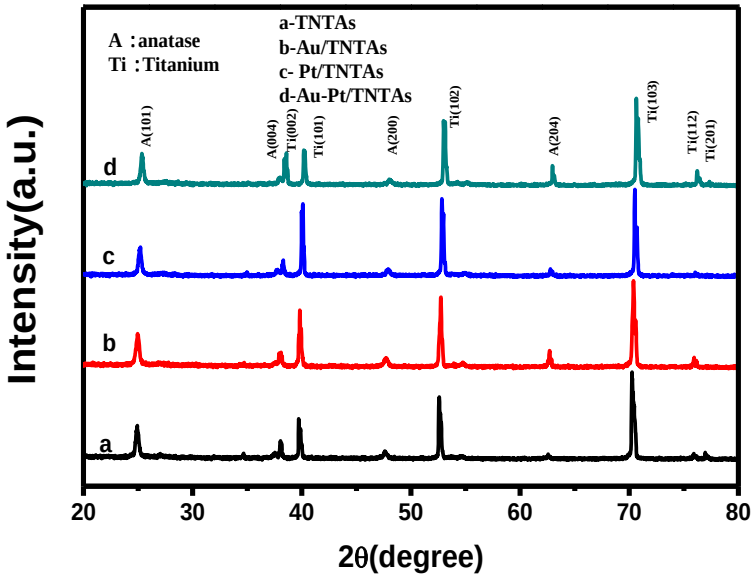

Figure 3. X-ray diffraction (XRD) patterns of the prepared (a) TNTAs, (b) Au/TNTAs, (c) Pt/TNTAs, and (d) Au-Pt/TNTAs.

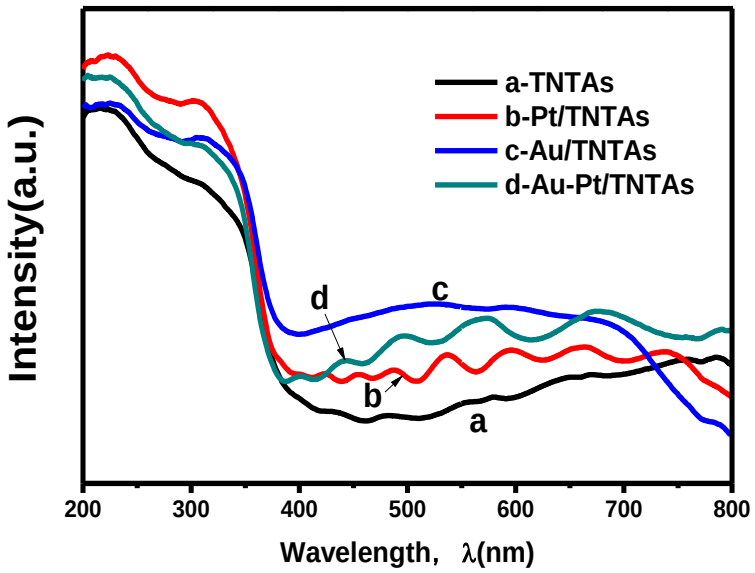

Figure 4. UV-vis DRS curves of the prepared (a) TNTAs, (b) Pt/TNTAs, (c) Au/TNTAs, (d) Au-Pt/TNTAs.

Figure 4 shows the DRS curves of the prepared TNTAs, Au/TNTAs, Pt/TNTAs and Au-Pt/TNTAs. It can be seen that the deposition of Au, Pt or Au-Pt nanoparticles had a significant effect on the spectral absorption properties of TNTAs. After the deposition of precious metal nanoparticles on the surface of TNTAs, the light absorption ability of the photocatalysts was slightly enhanced in the ultraviolet region but significantly enhanced in the visible region. This indicates that the presence of precious metal nanoparticles on the surface of TNTAs would enhance the light absorption ability of TNTAs, largely due to the surface plasma resonance (SPR) effect of the deposited precious nanoparticles [24, 25]. Meanwhile, the absorption band edge of the TNTAs sample was also red-

shifted to a longer wavelength, probably because of the bandgap structure change of TNTAs arising from the interaction between precious metal nanoparticles and the TNTAs [26].

In addition, the presence of precious metal nanoparticles on the TiO_2 surface can improve the ability to capture photogenerated carriers, and thus promote the separation of photogenerated carriers [27, 28]. The separation efficiency of photogenerated electron-hole pairs in a photocatalyst can be indirectly reflected from the PL emission spectra [29]. In general, the higher the PL emission intensity is, the higher the recombination rate of photogenerated carriers is [30-32].

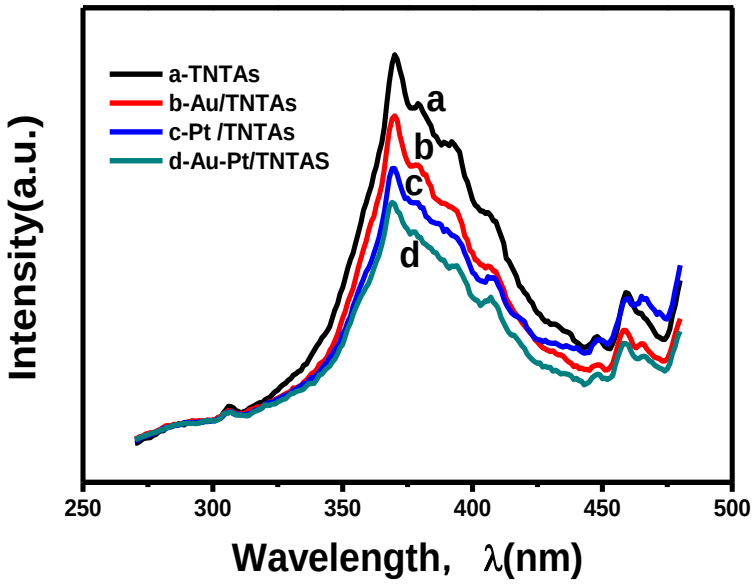

Figure 5. PL spectra of the prepared (a) TNTAs, (b) Au/TNTAs, (c) Pt/TNTAs, (d) Au-Pt/TNTAs.

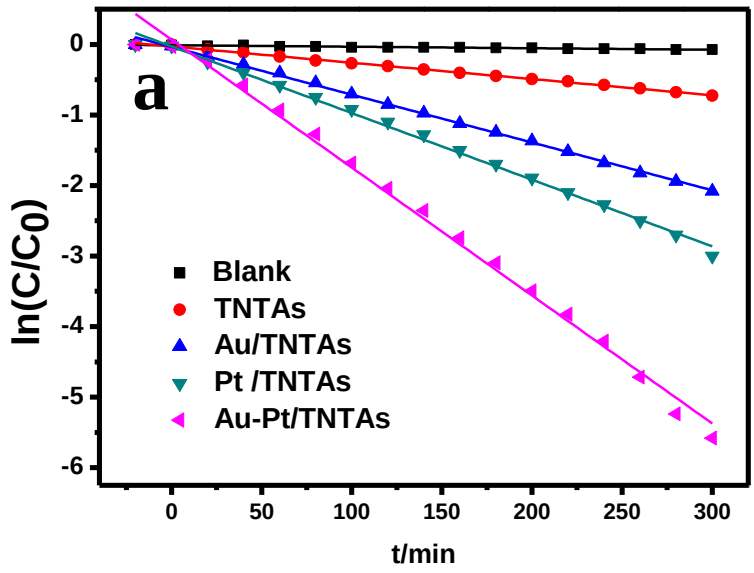

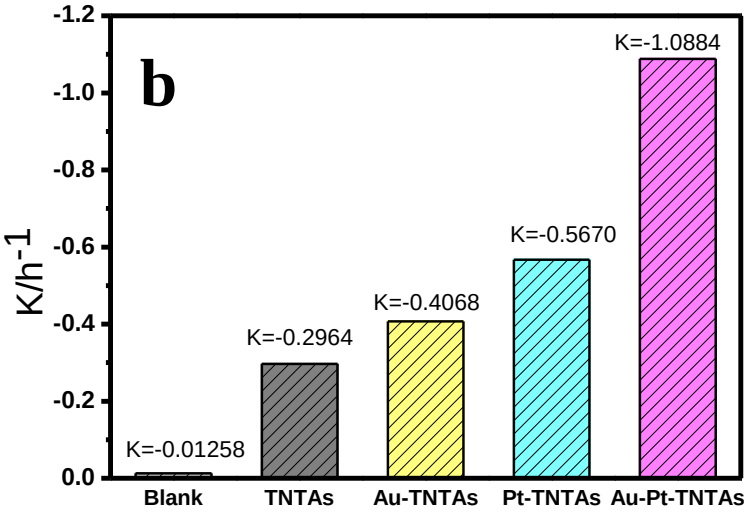

Figure 6. (a) The pseudo-first-order kinetics fitting data for photocatalytic degradation of RhB over the direct photolysis (Blank), TNTAs, Au/TNTAs, Pt/TNTAs, and Au-Pt/TNTAs under visible light irradiation($\lambda \geq 420$ nm); (b) A histogram for the RhB photodegradation rate constant (k) over the direct photolysis (Blank), TNTAs, Au/TNTAs, Pt/TNTAs, and Au-Pt/TNTAs.

Figure 5 shows the PL spectra of the prepared TNTAs, Au/TNTAs, Pt/TNTAs and Au-Pt/TNTAs. As shown, the PL intensities decreased in the order of TNTAs, Au/TNTAs, Pt/TNTAs and Au-Pt/TNTAs, indicating that the loading of noble metal nanoparticles could effectively suppress the recombination of photogenerated electrons and holes of the TNTAs. Apparently, the lowest PL intensity of the Au-Pt/TNTAs implies the lowest recombination rate of photogenerated electron-hole pairs, which would probably result in the enhanced photocatalytic performance.

Figure 6 shows the photocatalytic degradation curves of RhB over the prepared TNTAs, Au/TNTAs, Pt/TNTAs and Au-Pt/TNTAs under visible light ($\lambda \geq 420$ nm) irradiation. As seen, the self-degradation efficiency of RhB could be negligible, indicating its relatively good structural stability. For all the prepared photocatalysts, the photocatalytic degradation of RhB conformed to the pseudo-first-order reaction kinetic process, and could be applied to the following pseudo-first-order reaction kinetic equation [33-35]:

$$-ln\left(\frac{C}{C_0}\right) = k \times t$$

where C_0 and C are the concentrations of RhB at different irradiation time of t_0 and t, respectively, and k is the photocatalytic degradation pseudo-first-order rate constant (h^{-1}). According to the linear fitting curves of $\ln(C_0/C)$ versus irradiation time t (Figure 6a), the RhB degradation rate constant (k) could be calculated to be -0.01258, -0.2964, -0.4068, -0.5670, and -1.0884 h^{-1} for the blank sample, TNTAs, Au/TNTAs, Pt/TNTAs, and Au-Pt/TNTAs, respectively, as summarized in a histogram (Figure 6b). Obviously, the photocatalytic degradation activities of TNTAs were significantly improved after loading monometallic or bimetallic precious metals. Though the loading amount of Pt in the Pt/TNTAs sample was lower than that of Au in the Au/TNTAs, the photocatalytic degradation rate of Pt/TNTAs was higher than that of Au/TNTAs, suggesting that Pt nanoparticles possessed a higher co-catalytic activity than Au nanoparticles. Moreover, the degradation constant rate

of Au-Pt/TNTAs was much higher than that of Au/TNTAs or Pt/TNTAs, respectively, and was also greater than the sum of the latter two. Note that the photocatalytic performance of Au-Pt /TNTAs could be also comparable to or even higher than those of the previously-reported TiO_2-based photocatalysts [36-38].This confirms that the Au-Pt bimetallic loading had an apparent synergistic effect, thus leading to the significantly enhanced photocatalytic performance.

As discussed above, the loading of Au-Pt nanoparticles could effectively improve the photocatalytic activity of TNTAs. The improved photocatalytic activity of Au-Pt/TNTAs could be ascribed to the synergistic effect of Au-Pt cocatalyst. On the one hand, the optical absorption properties of Au-Pt/TNTAs could be enhanced on account of the surface plasma effect of Au-Pt nanoparticles. On the other hand, the Schottky heterojunction formed between the Au-Pt nanoparticles and TNTAs could promote the separation and migration of photogenerated carriers and inhibit the recombination process of photogenerated carriers. Thus, the above factors led to the improved photocatalytic performance of Au-Pt/TNTAs.

4. CONCLUSIONS

In summary, the Au-Pt bimetallic nanoparticles were successfully loaded on the surface of TNTAs to prepare the Au-Pt/TNTAs photocatalysts through a photoreduction approach, and the morphological structures and photocatalytic properties of the prepared Au-Pt/TNTAs were then explored. It was found that the Au-Pt bimetallic nanoparticles were well distributed on the surface of TNTAs. Compared with the TNTAs and the monometallic Au/TNTAs or Pt/TNTAs, the Au-Pt /TNTAs showed significantly improved photocatalytic activities for RhB degradation. The photocatalytic degradation rate constant of Au-Pt/TNTAs was much higher than those of TNTAs, Au/TNTAs and Pt/TNTAs, and was also greater than the sum of Au/TNTAs and Pt/TNTAs. The improved photocatalytic activity of Au-Pt /TNTAs could be attributed to the synergistic effect from the Au-Pt nanoparticles and TNTAs. On the one hand, the optical absorption ability of the Au-Pt/TNTAs could be largely improved on account of the surface plasma effect of precious metals. On the other hand, the Schottky heterojunction formed between the Au-Pt nanoparticles and TNTAs would promote the separation and migration process of photogenerated carriers and thus inhibit the recombination process of photogenerated carriers. As a result, the photocatalytic activities of Au-Pt/TNTAs were ultimately improved to a large extent. This work is of much significance for guiding the design of highly efficient bimetallic precious metals-loaded photocatalysts and deepening the understanding of their corresponding photocatalytic mechanism.

ACKNOWLEDGEMENTS

The authors gratefully acknowledge the financial supports from the Zhejiang Provincial Natural Science Foundation of China (No. LY19E020003, LQ20F040007, LQ19F040004), National Natural Science Foundation of China (No. 51972294, 51872271).

References

1. R. Shwetharani, M. Sakar, C.A.N. Fernando, V. Binas and R.G. Balakrishna, *Catal. Sci. Technol.*, 9 (2019) 12.
2. M. Pelaez, N.T. Nolan, S.C. Pillai, M.K. Seery, P. Falaras, A.G. Kontos, P.S.M. Dunlop, J.W.J. Hamilton, J.A. Byrne, K. O'Shea, M.H. Entezari and D.D. Dionysiou, *Appl. Catal. B: Environ.*, 125 (2012) 331.
3. J.X. Low, B. Cheng and J.G. Yu, *Appl. Surf. Sci.*, 392 (2017) 658.
4. K. Nakata and A. Fujishima, *J. Photochem. Photobiol. C-Photochem. Review*, 13 (2012) 169.
5. G.K. Mor, O.K. Varghese, M. Paulose, K. Shankar and C.A. Grimes, *Sol. Energy Mater. Sol. Cells*, 90 (2006) 2011.
6. A.E.R. Mohamed and S. Rohani, *Energy Environ. Sci.*, 4 (2011) 1065.
7. Q.X. Zhou, Z. Fang, J. Li and M.Y. Wang, *Micropor. Mesopor. Mater.*, 202 (2015) 22.
8. J.M. Macak, H. Tsuchiya, A. Ghicov and P. Schmuki, *Electrochem. Commun.*, 7 (2005) 1133.
9. K. Shankar, J. Bandara, M. Paulose, H. Wietasch, O.K. Varghese, G.K. Mor, T.J. LaTempa, M. Thelakkat and C.A. Grimes, *Nano Lett.*, 8 (2008) 1654.
10. L. Sun, J. Li, C.L. Wang, S.F. Li, H.B. Chen and C.J. Lin, *Sol. Energy Mater. Sol. Cells*, 93 (2009) 1875.
11. Y. Jing, X.M. Hu and C.Y. Shao, *Int. J. Electrochem. Sci.*, 12 (2017) 9311.
12. H. Chen, S. Chen, X. Quan, H.T. Yu, H.M. Zhao and Y.B. Zhang, *J. Phys. Chem. C*, 112 (2008) 9285.
13. Q.L. Huang, T. Gao, F. Niu, D. Chen, Z. Chen, L.S. Qin, X.G. Sun, Y.X. Huang and K.Y. Shu, *Superlattice Microstruct.*, 75 (2014) 890.
14. A. Gallo, M. Marelli, R. Psaro, V. Gombac, T. Montini, P. Fornasiero, R. Pievo and V. Dal Santo, *Green Chem.*, 14 (2012) 330.
15. M. Nischk, P. Mazierski, Z.S. Wei, K. Siuzdak, N.A. Kouame, E. Kowalska, H. Remita and A. Zaleska-Medynska, *Appl. Surf. Sci.*, 387 (2016) 89.
16. J.B. Priebe, J. Radnik, C. Kreyenschulte, A.J.J. Lennox, H. Junge, M. Beller and A. Bruckner, *ChemCatChem*, 9 (2017) 1025.
17. R.S. Moakhar, M. Jalali, A. Kushwaha, G.K.L. Goh, N. Riahi-Noori, A. Dolati and M. Ghorbani, *J. Appl. Electrochem.*, 48 (2018) 995.
18. X.J. Zhang, F. Han, B. Shi, S. Farsinezhad, G.P. Dechaine and K. Shankar, *Angew. Chem. Int. Ed.*, 51 (2012) 12732.
19. H. Eskandarloo, M. Hashempour, A. Vicenzo, S. Franz, A. Badiei, M.A. Behnajady and M. Bestetti, *Appl. Catal. B: Environ.*, 185 (2016) 119.
20. J.M. Macak, H. Hildebrand, U. Marten-Jahns and P. Schmuki, *J. Electroanal. Chem.*, 621 (2008) 254.
21. S. Jo, P. Verma, Y. Kuwahara, K. Mori, W. Choi and H. Yamashita, *J. Mater. Chem. A*, 5 (2017) 21883.
22. J.J. Lin, T. Sun, M.B. Li, J.X. Yang, J.N. Shen, Z.Z. Zhang, Y. Wang, X.Y. Zhang and X.X. Wang, *J. Catal.*, 372 (2019) 8.
23. Z.J. Hu, D. Chen, X.Q. Zhan, F. Wang, L.S. Qin and Y.X. Huang, *Appl. Phys. A*, 123 (2017) 399.
24. L.Q. Liu, S.X. Ouyang and J.H. Ye, *Angew. Chem. Int. Ed.*, 52 (2013) 6689.
25. F. Niu, D. Chen, L.S. Qin, T. Gao, N. Zhang, S. Wang, Z. Chen, J.Y. Wang, X.G. Sun and Y.X. Huang, *Sol. Energy Mater. Sol. Cells*, 143 (2015) 386.
26. V. Vaiano, C.A. Jaramillo-Paez, M. Matarangolo, J.A. Navio and M.D. Hidalgo, *Mater. Res. Bull.*, 112 (2019) 251.
27. W. Zhou, T. Li, J.Q. Wang, Y. Qu, K, Pan, Y. Xie, G.H. Tian, L. Wang, Z.Y. Ren, B.J. Jiang and H.G. Fu, *Nano Res.*, 7 (2014) 731.
28. Z.Y. Zhang, Z. Wang, S.W. Cao and C. Xue, *J. Phys. Chem. C*, 117 (2013) 25939.
29. B.S. Liu, X.J. Zhao, J.G. Yu, I.P. Parkins, A. Fujishima and K. Nakata, *J. Photochem. Photobiol.*

C: Photochem. Rev., 39 (2019) 1.
30. X.Z. Li and F.B. Li, *Chemosphere,* 48 (2002) 1103.
31. W. Zhao, Y. Wang, Y. Yang, J. Tang and Y. Yang, *Appl. Catal. B: Environ.*, 115 (2012) 90.
32. X. Liu, Z. Li, C. Zhao, W. Zhao, J. Yang, Y. Wang and F. Li, *J. Colloid Interface Sci.,* 419 (2014) 9.
33. N. Zhang, D. Chen, F. Niu, S. Wang, L.S. Qin and Y.X. Huang, *Sci. Rep.*, 6 (2016) 26467.
34. Y.M. Shen, F. Li, S.F. Li, D.B. Liu, L.H. Fan and Y. Zhang, *Int. J. Electrochem. Sci.,* 7 (2012) 8702.
35. J.C. Yu, J.G. Yu, W.K. Ho, Z.T. Jiang and L.Z. Zhang, *Chem. Mater.*, 14 (2002) 3808.
36. L.L. Lai, W. Wen and J.M. Wu, *CrystEngComm,,* 18 (2016) 5195.
37. J. Wu, K. Zhu, Y.F. Guo, H. Xu and W. Yan, *Int. J. Electrochem. Sci.*, 15 (2020) 1091.
38. L.L. Qiu, Z.D. Chu, S.L. Yang, Y. Chen, L.X. Song, P.F. Du and J. Xiong, *J. Nanosci. Nanotechnol.,* 19 (2019) 5723.